Palmitic acid dysregulates the Hippo–YAP pathway and inhibits angiogenesis by inducing mitochondrial damage and activating the cytosolic DNA sensor cGAS–STING–IRF3 signaling mechanism

Received for publication, June 27, 2017 Published, Papers in Press, July 11, 2017, DOI 10.1074/jbc.M117.804005

Liangshuai Yuan[‡], **Yun Mao**[‡§¶‖], **Wei Luo**[‡§¶‖], **Weiwei Wu**[‡], **Hao Xu**[‡], **Xing Li Wang**[‡§¶‖1], **and Ying H. Shen**[§¶‖2]

From the [‡]*Shandong University Qilu Hospital Research Center for Cell Therapy, Key Laboratory of Cardiovascular Remodeling and Function Research, the* [§]*Qilu Hospital of Shandong University, Jinan 250012, China, the* [¶]*Department of Surgery, Baylor College of Medicine, Houston, Texas 70030, and the* [‖]*Department of Surgery, Texas Heart Institute, Houston, Texas 70030*

Edited by Xiao-Fan Wang

Impaired angiogenesis and wound healing carry significant morbidity and mortality in diabetic patients. Metabolic stress from hyperglycemia and elevated free fatty acids have been shown to inhibit endothelial angiogenesis. However, the underlying mechanisms remain poorly understood. In this study, we show that dysregulation of the Hippo–Yes-associated protein (YAP) pathway, an important signaling mechanism in regulating tissue repair and regeneration, underlies palmitic acid (PA)-induced inhibition of endothelial angiogenesis. PA inhibited endothelial cell proliferation, migration, and tube formation, which were associated with increased expression of mammalian Ste20-like kinases 1 (MST1), YAP phosphorylation/inactivation, and nuclear exclusion. Overexpression of YAP or knockdown of MST1 prevented PA-induced inhibition of angiogenesis. When searching upstream signaling mechanisms, we found that PA dysregulated the Hippo–YAP pathway by inducing mitochondrial damage. PA treatment induced mitochondrial DNA (mtDNA) release to cytosol, and activated cytosolic DNA sensor cGAS–STING–IRF3 signaling. Activated IRF3 bound to the *MST1* gene promoter and induced MST1 expression, leading to MST1 up-regulation, YAP inactivation, and angiogenesis inhibition. Thus, mitochondrial damage and cytosolic DNA sensor cGAS–STING–IRF3 signaling are critically involved in PA-induced Hippo–YAP dysregulation and angiogenesis suppression. This mechanism may have implication in impairment of angiogenesis and wound healing in diabetes.

Delayed wound healing and diabetic skin ulcer are major complications of diabetes that cause significant disability and mortality in these patients (1–3). Wound healing is a complex process of coagulation, inflammation, angiogenesis, tissue repair, and remodeling. The process involves proliferation, migration, and functions of multiple cells including stem cells, endothelial cells, fibroblasts, and keratinocytes (4–6). Abnormalities in these cells (2), particularly endothelial cells (7–9), have been implicated in the impaired wound healing in diabetes. Metabolic stress produced by hyperglycemia (10–13) and elevated free fatty acids (14) has been shown to inhibit angiogenesis and wound healing. However, the underlying mechanisms remain poorly understood.

The Hippo pathway (15–19) and its effector Yes-associated protein (YAP)[3] (20) are important in regulating organ growth, tissue repair, and regeneration. The Hippo pathway contains mammalian Ste20-like kinases 1/2 (MST1/2), Salvador (SAV), and large tumor suppressor (LATS1/2). YAP and the transcriptional coactivator with PDZ-binding motif (TAZ) are the primary downstream effectors of the Hippo pathway (15–20). MST1/2 phosphorylates and activates LATS1/2, (15, 20), which in turn phosphorylates YAP at Ser-127 or Ser-381, leading to its cytoplasmic retention and degradation, and subsequent transcription suppression of its target genes (15–18). YAP promotes cell proliferation, survival, and angiogenesis (20–22). The Hippo pathway, by inactivating YAP, inhibits cell survival, proliferation, and angiogenesis (15, 17, 18, 20–22). The Hippo pathway and YAP are key regulators in angiogenesis (21, 22) and wound healing (23).

Given the importance of the Hippo–YAP pathway in angiogenesis, we hypothesized that dysregulation of this pathway is involved in metabolic stress-induced inhibition of endothelial angiogenesis. In the current study, we found that palmitic acid (PA) induced MST1 expression, and subsequently suppressed YAP and endothelial angiogenesis. PA induced MST1 expression through the induction of mitochondrial

This work was supported by 973 National Basic Research Program of China Grant 2014CB542401 (to X. L. W.), National Institutes of Health Grant 1R01HL131980-01 (to Y. H. S.), American Heart Association Grant 15GRNT23040007 (to Y. H. S.), and the Shandong University National Qianren Scholar Fund (to X. L. W.). The authors declare that they have no conflicts of interest with the contents of this article. The content is solely the responsibility of the authors and does not necessarily represent the official views of the National Institutes of Health.

This article contains supplemental Figs. S1 and S2 and Table S1.

[1] To whom correspondence may be addressed: No. 107, Wenhua West Rd., Qilu Hospital, Jinan 250012, Shandong, China. E-mail: xingliwang@sdu.edu.cn.

[2] To whom correspondence may be addressed: BM390, Baylor College of Medicine, One Baylor Plaza, TX 77030. Tel.: 832-355-9952; Fax: 832-355-9951; E-mail: hyshen@bcm.edu.

[3] The abbreviations used are: YAP, Yes-associated protein; PA, palmitic acid; MST1, mammalian Ste20-like kinases 1; mtDNA mitochondrial DNA; cGAS, cyclic GMP-AMP synthase; STING, stimulator of interferon genes; IRF3, interferon regulatory factor 3; HAEC, human aortic endothelial cell; CCCP, carbonyl cyanide *m*-chlorophenyl hydrazone.

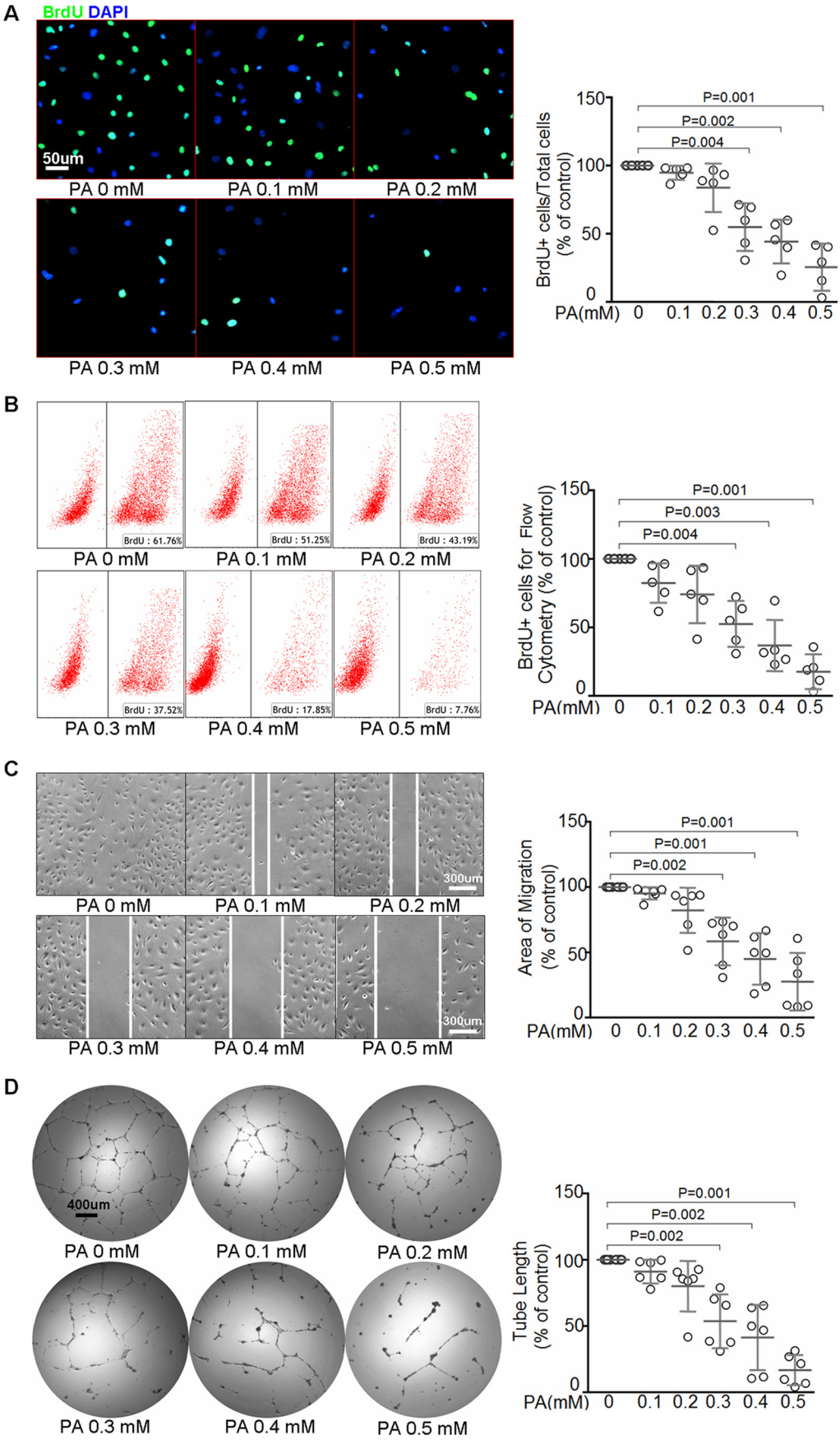
A
BrdU DAPI
50um
PA 0 mM
PA 0.1 mM
PA 0.2 mM
PA 0.3 mM
PA 0.4 mM
PA 0.5 mM
BrdU+ cells/Total cells (% of control)
P=0.001
P=0.002
P=0.004
PA(mM) 0 0.1 0.2 0.3 0.4 0.5
B
BrdU : 61.76%
BrdU : 51.25%
BrdU : 43.19%
BrdU : 37.52%
BrdU : 17.85%
BrdU : 7.76%
BrdU+ cells for Flow Cytometry (% of control)
P=0.001
P=0.003
P=0.004
C
300um
Area of Migration (% of control)
P=0.001
P=0.001
P=0.002
D
400um
Tube Length (% of control)
P=0.001
P=0.002
P=0.002

damage and mitochondrial DNA release, and activation of the cytosolic DNA sensor cyclic GMP-AMP synthase (cGAS)–interferon genes protein (STING)–interferon regulatory factor 3 (IRF3) pathway.

Results

Palmitic acid inhibits endothelial proliferation, migration, and angiogenesis

To examine the effects of metabolic stress on endothelial angiogenesis, we treated human aortic endothelial cells (HAECs) with PA, the main type of free fatty acid in metabolic syndrome (24). We found that high concentrations of PA significantly reduced endothelial proliferation (Fig. 1, *A* and *B*) and impaired endothelial migration (Fig. 1*C*). HAECs were able to form tubules spontaneously. However, PA treatment severely destroyed tube formation, indicating angiogenesis deficiency (Fig. 1*D*). These findings suggest that PA inhibits endothelial proliferation, migration, and angiogenesis.

Palmitic acid activates MST1 and inhibits YAP

We next examined whether PA-induced inhibition of angiogenesis was associated with dysregulation of the Hippo–YAP pathway. As shown in Fig. 2*A*, PA induced MST1 expression and phosphorylation, indicative of MST1 activation. Consistently, PA induced YAP phosphorylation (Fig. 2*A*) and nucleus exclusion (Fig. 2*B*), indicating its inactivation. Overexpression of wild type (WT) YAP not only promoted basal endothelial proliferation (Fig. 2*C*) and tube formation (Fig. 2*D*), but also prevented PA-induced reduction in endothelial proliferation (Fig. 2*C*) and tube formation (Fig. 2*D*). Overexpression of constitutively active YAP S127A mutant, in which mutation of the phosphorylation site in YAP results in its resistance to phosphorylation and inactivation (25), also exhibited protective effects (Fig. 2, *C* and *D*). In contrast, knocking down YAP with siRNA (supplemental Figs. S1*A* and S2*A*) not only reduced endothelial proliferation (supplemental Fig. S1, *B* and *C*) and tube formation (supplemental Fig. S1*D*) at basal conditions, but also amplified PA-induced inhibition of endothelial proliferation (supplemental Fig. S1, *B* and *C*) and tube formation (supplemental Fig. S1*D*). These results indicate that YAP inactivation underlies PA-induced inhibition of endothelial proliferation and angiogenesis.

MST1 is involved in palmitic acid-induced inhibition of endothelial angiogenesis

We then investigated the role of MST1 in the inhibition of YAP and endothelial angiogenesis. Knocking down MST1 (supplemental Fig. S2*B*) prevented PA-induced YAP phosphorylation (Fig. 3*A*) and cytoplasm retention (Fig. 3*B*). Additionally, silencing MST1 promoted endothelial proliferation at basal levels, and prevented PA-induced inhibition of endothelial proliferation (Fig. 3, *C* and *D*). Similarly, knocking down MST1 alleviated PA-induced inhibition of tube formation (Fig. 3*E*). Together, these results suggest that MST1 is involved in PA-induced inactivation of YAP and impairment of endothelial angiogenesis.

PA induces mitochondrial DNA release to cytosol and activates the cytosolic DNA sensor cGAS–STING–IRF3 pathway

We further studied the mechanism by which PA activated MST1 and inhibited YAP and endothelial angiogenesis. One of the significant adverse effects of free fatty acid oversupply is mitochondrial damage that can trigger cell dysfunction and even cell death (26, 27). Our recent study suggests that PA can cause mitochondrial damage and cytosolic release of mitochondria DNA (mtDNA) (28). Through cGAS (29–31), cytosolic DNA including cytosolic mtDNA can be converted to second messenger cGAMP that activates DNA sensor STING–IRF3 signaling (32, 33), leading to transcription of proinflammatory molecules and activation of inflammatory response. cGAS–STING–IRF3 signaling has been shown to mediate mitochondrial damage-induced inflammatory response (28) and cell dysfunction (34–36). We asked whether this mechanism also mediated PA-induced angiogenesis suppression.

We first confirmed the effects of PA on mitochondrial function by measuring mitochondrial membrane potential ($\Delta\psi_m$) using tetraethylbenzimidazolylcarbocyanine iodide (JC-1) staining. JC-1 is a cationic fluorescent dye that forms red aggregates in polarized functional mitochondria and stays as a green monomer outside depolarized mitochondria. We observed that PA treatment decreased red aggregates and increased green monomers with an increased green/red fluorescence ratio (Fig. 4*A*), indicating reduction in $\Delta\psi_m$ and mitochondrial dysfunction. Additionally, co-staining of double strand DNA (dsDNA) and mitochondria (MitoTracker) showed that PA treatment significantly increased cytosolic dsDNA (dsDNA that did not co-localize with either mitochondria or the nucleus) (28) (Fig. 4*B*). Further cytosolic mtDNA analysis (by PCR of cytosolic DNA with mtDNA sequences as primers) showed PA significantly increased cytosolic mtDNA (Fig. 4*C*). Furthermore, prolonged PA treatment increased the levels of cGAS, STING, phosphorylated IRF3 (Fig. 4*D*), suggesting activation of the cGAS–STING–IRF3 pathway. The up-regulation of cGAS–STING–IRF3 was associated with increased MST1 protein and YAP phosphorylation/inactivation (Fig. 4*D*).

Finally, inducing mitochondrial damage with carbonyl cyanide *m*-chlorophenyl hydrazone (CCCP), an agent that increases mitochondrial permeability and damage, increased levels of cGAS, STING, and phosphorylated IRF3 (Fig. 4*E*), and stimulated STING perinuclear translocation and IRF3 nuclear translocation (Fig. 4*F*), indicating a direct effect of mitochondrial damage in cGAS–STING–IRF3 activation. Together, these data suggest that PA treatment and mitochondrial

Figure 1. Palmitic acid inhibits endothelial proliferation, migration, and angiogenesis. HAECs were treated with different concentrations of PA for 24 h before the following analysis. Representative images of BrdU staining ($n = 5$ biological repeats) (*A*) and flow cytometry analysis of the BrdU proliferation assay ($n = 5$ biological repeats) (*B*) showed that PA treatment induced a dose-dependent inhibition of endothelial cell proliferation. *C,* scratch assay showed that PA treatment induced a dose-dependent inhibition of endothelial cell migration ($n = 6$ biological repeats). *D,* Matrigel tube formation assay showed that PA reduced endothelial cell tube formation ($n = 6$ biological repeats).

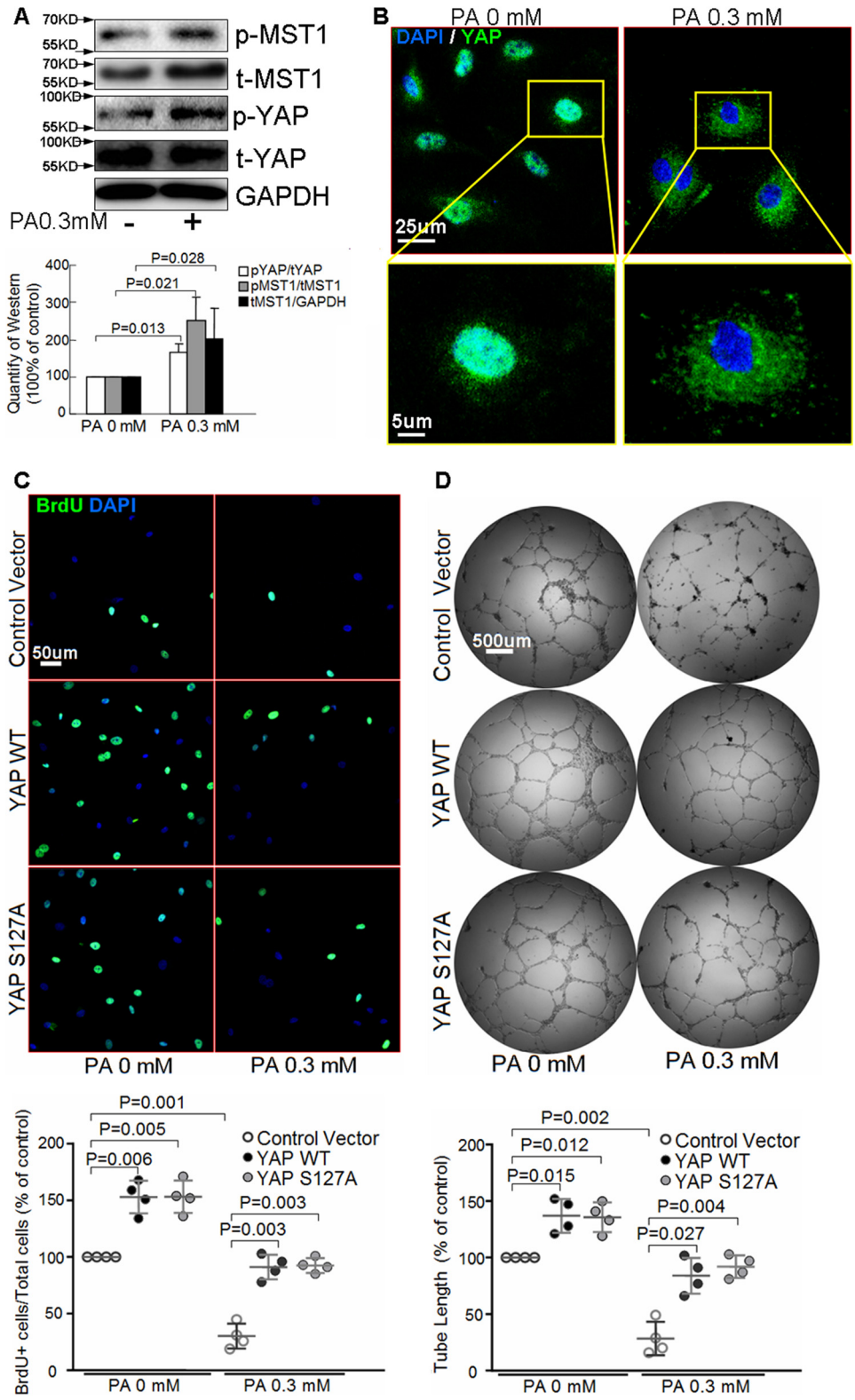

Figure 2. Palmitic acid up-regulates MST1 and inhibits YAP. *A* and *B*, HAECs were treated with PA for 24 h. Western blot analysis showed that PA induced MST1 expression and phosphorylation, and YAP phosphorylation ($n = 6$ biological repeats) (*A*). Representative images of immunostaining showed that PA prevented YAP nuclear translocation ($n = 6$ biological repeats) (*B*). *C* and *D*, HAECs were transfected with the YAP mutation plasmid (YAP S127A) or wild type plasmid (*WT*), followed by PA treatment for 24 h. Representative images of BrdU analysis showed that overexpression of YAP WT or YAP S127A increased endothelial cell proliferation ($n = 4$ biological repeats) (*C*). *In vitro* tube formation assay showed that overexpression of YAP WT or YAP S127A enhanced endothelial tube formation ($n = 4$ biological repeats) (*D*).

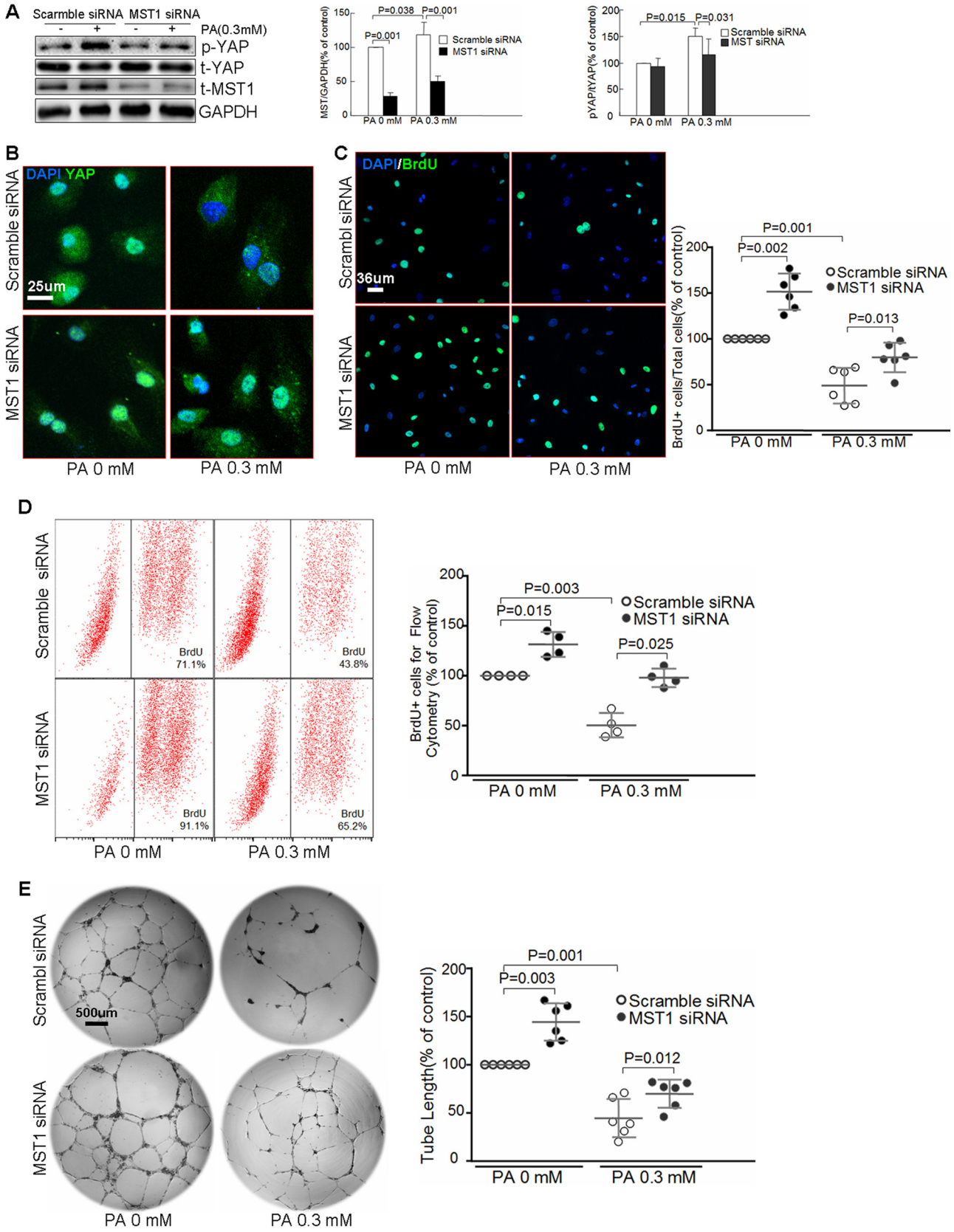

Figure 3. MST1 is involved in palmitic acid-induced inhibition of endothelial proliferation and angiogenesis. HAECs were transfected with scramble siRNA or MST1 siRNA and then treated with PA for 24 h. *A,* Western blot analysis showed that silencing MST1 inhibited PA-induced YAP phosphorylation. (n = 6 biological repeats). *B,* representative images of immunostaining showed that knocking down MST1 prevented the PA-induced YAP cytoplasm retention (n = 6 biological repeats). Representative images of BrdU staining (n = 6 biological repeats) (*C*) and flow cytometry analysis of the BrdU proliferation assay (n = 4 biological repeats) (*D*) showed that silencing MST1 prevented PA-induced inhibition of endothelial proliferation. *In vitro* tube formation assay showed that MST1 siRNA treatment partially reversed PA-induced impairment of endothelial tube formation (n = 6 biological repeats) (*E*).

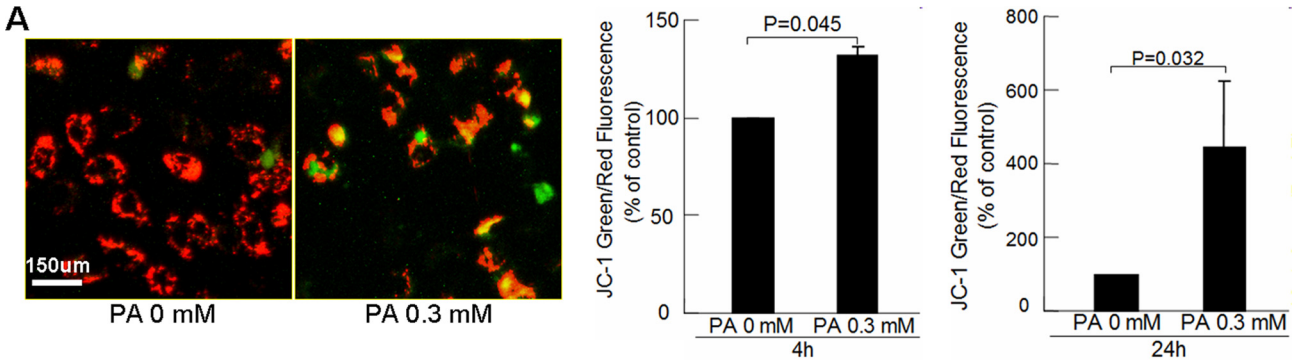
A
150um
PA 0 mM
PA 0.3 mM
JC-1 Green/Red Fluorescence (% of control)
P=0.045
PA 0 mM
PA 0.3 mM
4h
P=0.032
24h

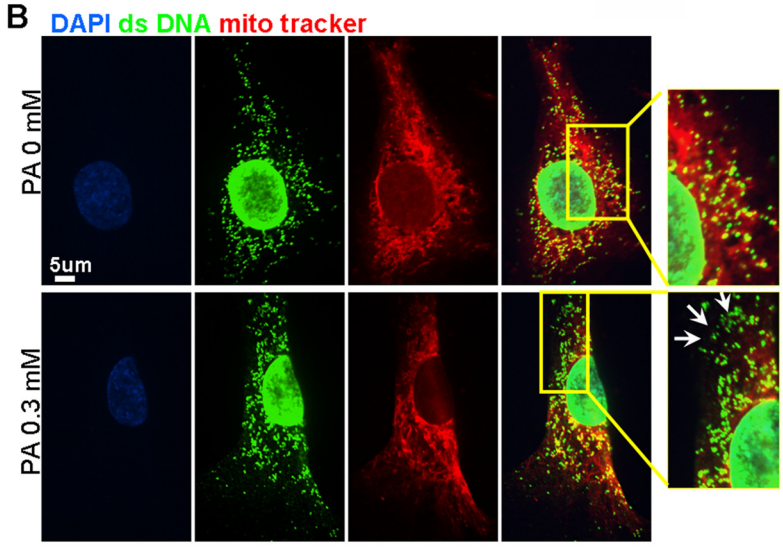
B
DAPI ds DNA mito tracker
PA 0 mM
PA 0.3 mM
5um

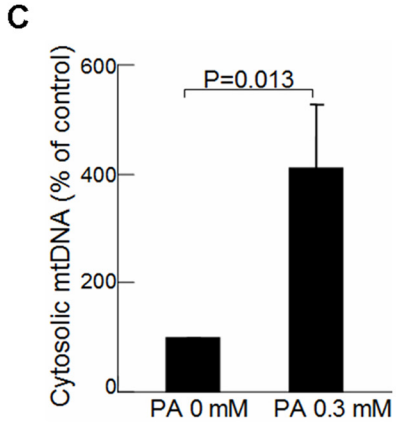
C
Cytosolic mtDNA (% of control)
P=0.013
PA 0 mM
PA 0.3 mM

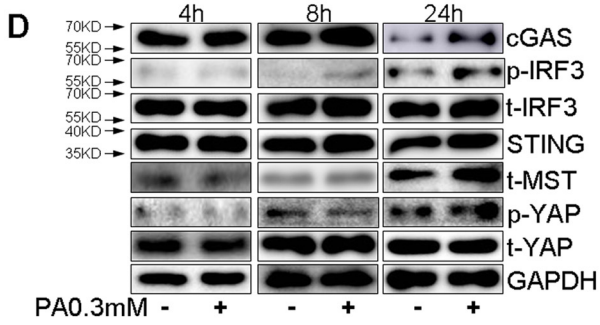
D
4h
8h
24h
cGAS
p-IRF3
t-IRF3
STING
t-MST
p-YAP
t-YAP
GAPDH
PA0.3mM

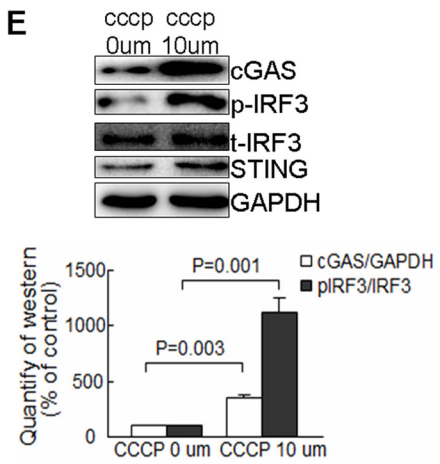
E
cccp 0um
cccp 10um
cGAS
p-IRF3
t-IRF3
STING
GAPDH
Quantify of western (% of control)
P=0.001
P=0.003
cGAS/GAPDH
pIRF3/IRF3
CCCP 0 um
CCCP 10 um

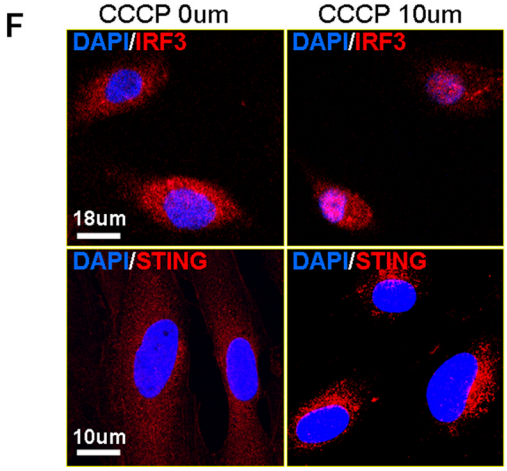
F
CCCP 0um
CCCP 10um
DAPI/IRF3
18um
DAPI/STING
10um

damage can result in cytosolic release of mtDNA and activation of cytosolic DNA sensor cGAS–STING–IRF3 signaling, which are associated with dysregulation of the Hippo–YAP pathway.

DNA sensor cGAS–STING–IRF3 signaling mediates PA-induced Hippo–YAP dysregulation

We further examined the involvement of the cGAS–STING–IRF3 pathway in the regulation of MST1 and YAP. Silencing cGAS (supplemental Fig. S2*C*) with siRNA inhibited PA-induced IRF3 phosphorylation, MST1 expression, and YAP phosphorylation (Fig. 5*A*), suggesting the involvement of cGAS in STING–IRF3 activation and Hippo–Yap dysregulation. Similarly, knocking down STING and IRF3 (supplemental Fig. S2, *E* and *F*) prevented PA-induced MST1 expression and YAP phosphorylation (Fig. 5*B*), and YAP cytosolic retention (Fig. 5*C*). These results indicate that the cGAS–STING–IRF3 pathway is critical to PA-induced MST1 up-regulation and YAP inhibition in endothelial cells.

IRF3 directly binds to MST1 promoter and mediates PA-induced induction of MST1 expression

We then asked how the cGAS–STING–IRF3 pathway regulates the Hippo–YAP pathway. It has been shown that activated MST1 promotes immune reaction and inflammatory response (38, 39). Because IRF3 induces the transcription of proinflammatory factors (40), we asked whether IRF3 also promoted MST1 expression. Indeed, silencing STING and IRF3 with specific siRNA reduced PA-induced MST1 mRNA (Fig. 6*A*), suggesting that IRF3 regulates MST1 at the mRNA level. Sequencing analysis of the *MST1* promoter revealed putative IRF3-binding sites in the 5′ untranslated region (Fig. 6*B*) of the *MST1* gene. Chromatin immunoprecipitation assay showed that IRF3 bound to the *MST1* promoter (Fig. 6*C*), and this binding was enhanced by treating cells with PA or CCCP. Together, these findings suggest that IRF3 directly binds to the *MST1* promoter and promotes MST1 expression in response to PA challenge and mitochondrial damage.

The cGAS–STING–IRF3 pathway is involved in PA-induced inhibition of endothelial angiogenesis

Finally, we show that silencing cGAS, STING, and IRF3 promoted endothelial proliferation at basal levels, and partially prevented PA-induced inhibition of endothelial proliferation (Fig. 7, *A* and *B*). Similarly, knocking down cGAS, STING, and IRF3 improved endothelial tube formation and reversed PA-induced impairment of endothelial angiogenesis (Fig. 7*C*). Together, these findings suggest a critical role of the cGAS–STING–IRF3 pathway in PA-induced inhibition of endothelial proliferation and angiogenesis.

Discussion

In this study, we show that PA dysregulates the Hippo–YAP pathway and inhibits angiogenesis. PA induces mitochondrial damage and cytosolic release of mtDNA, which activates the cytosolic DNA sensor cGAS–STING–IRF3 pathway. Activated IRF3 binds to the *MST1* promoter and induces MST1 expression, leading to YAP phosphorylation/inactivation and angiogenesis suppression (Fig. 7*D*).

Although impaired angiogenesis and wound healing in diabetes is widely reported, the pathogenesis remains incomplete understood. Hippo–YAP (16, 22) signaling is a key pathway in regulating tissue repair and angiogenesis. YAP, by inducing the expression of proangiogenic factors (22) and epithelial-to-mesenchymal transition (41) promotes angiogenesis (21, 22). In contrast, the Hippo pathway, by inactivating YAP, inhibits angiogenesis and tissue repair (42). Here we show that dysregulation of Hippo–YAP signaling is also responsible for PA-induced inhibition of angiogenesis. PA treatment activated MST1 and subsequently inhibited YAP, leading to the inhibition of endothelial proliferation and tube formation. This finding implies that dysregulation of Hippo–YAP may represent an important mechanism underlying impaired angiogenesis and wound healing in diabetes.

Several triggers and molecules such as reactive oxygen species (43, 44), thioredoxin-interacting protein (13), and protein-tyrosine phosphatase 1B (45) have been implicated in the inhibition of angiogenesis in diabetes. Mitochondrial dysfunction and damage are significant features in diabetes (46, 47). Mitochondrial damage induced by metabolic stress (48) triggers endothelial dysfunction and injury, contributing to the development of cardiovascular diseases (48–50). Here we show that mitochondrial damage is an important mechanism responsible for PA-induced angiogenesis inhibition. We show that PA-induced mtDNA release to cytosol, which may activate cytosolic DNA sensor cGAS–STING–IRF3 signaling, leading to up-regulation of MST1 and inhibition of YAP and angiogenesis. Thus, mitochondrial damage, in addition to inducing endothelial dysfunction and inflammation, can also inhibit endothelial angiogenesis. Protecting mitochondria from damage and/or promoting the removal of damaged mitochondria may be critical in preserving endothelial angiogenesis capacity.

The Hippo–YAP pathway can be regulated by multiple mechanisms such as cell–cell interaction and mechanical signals, and by various signaling pathways (25). Although pathways such as PI3-kinase signaling activate YAP (51), tumor suppressors activate the Hippo pathway and inactivate YAP (52, 53). Here, we identified a new signaling pathway, the proinflammatory DNA sensor cGAS–STING–IRF3 pathway as a trigger

Figure 4. PA induces mtDNA release to cytosol and activates the cytosolic DNA sensor cGAS–STING–IRF3 pathway. *A–C,* HAECs were treated with PA for 4 or 24 h. *A,* representative images and quantification of JC-1 staining showed that PA treatment induced mitochondrial depolarization ($n = 4$, biological repeats). *B,* double staining of mitochondria (MitoTracker) and double strand DNA (dsDNA) showed that PA triggered dsDNA release to cytosol (*white arrows*, dsDNA that did not co-localize with either mitochondria or the nucleus) ($n = 6$ biological repeats). *C,* PCR analysis of mtDNA in cytosolic fractions showed that PA treatment increased cytosolic mtDNA ($n = 4$ biological repeats). *D,* Western blot analysis showed that PA activated cGAS, STING, IRF3, and MST1 ($n = 3$ biological repeats). *E* and *F,* HAECs were treated with CCCP for 24 h. Western blot analysis showed up-regulation of cGAS, STING, and IRF3 by CCCP treatment ($n = 6$ biological repeats) (*E*). Representative images of immunostaining showed that CCCP treatment induced STING perinuclear translocation and IRF3 nuclear translocation ($n = 4$ biological repeats) (*F*).

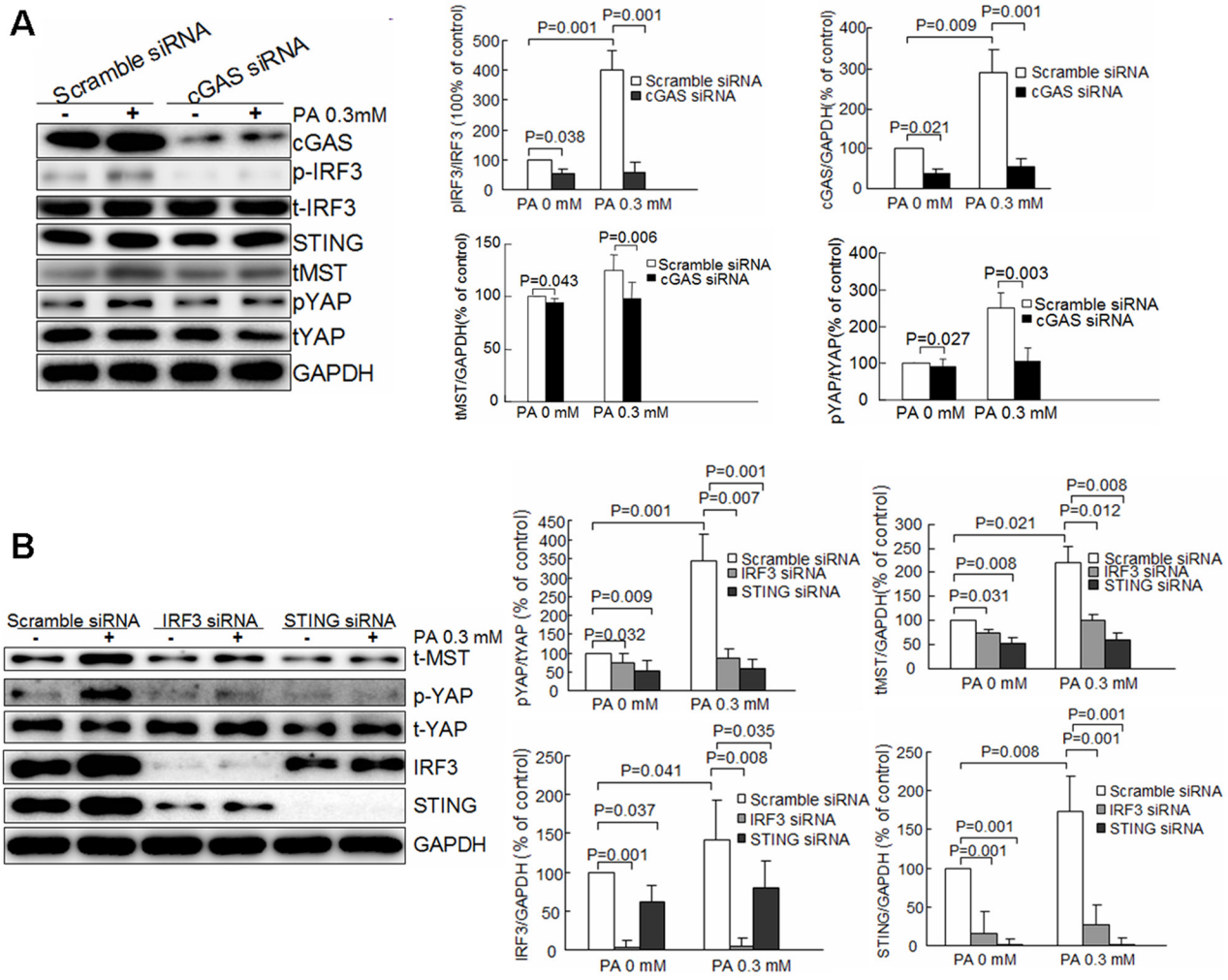
A
Scramble siRNA
cGAS siRNA
PA 0.3mM
cGAS
p-IRF3
t-IRF3
STING
tMST
pYAP
tYAP
GAPDH
pIRF3/IRF3 (100% of control)
cGAS/GAPDH(% of control)
tMST/GAPDH(% of control)
pYAP/tYAP(% of control)
Scramble siRNA
cGAS siRNA
PA 0 mM
PA 0.3 mM
B
Scramble siRNA
IRF3 siRNA
STING siRNA
PA 0.3 mM
t-MST
p-YAP
t-YAP
IRF3
STING
GAPDH
pYAP/tYAP (% of control)
tMST/GAPDH(% of control)
IRF3/GAPDH (% of control)
STING/GAPDH (% of control)
C
YAP DAPI
Scramble siRNA
IRF3 siRNA
STING siRNA
50um
PA 0 mM
PA 0.3 mM

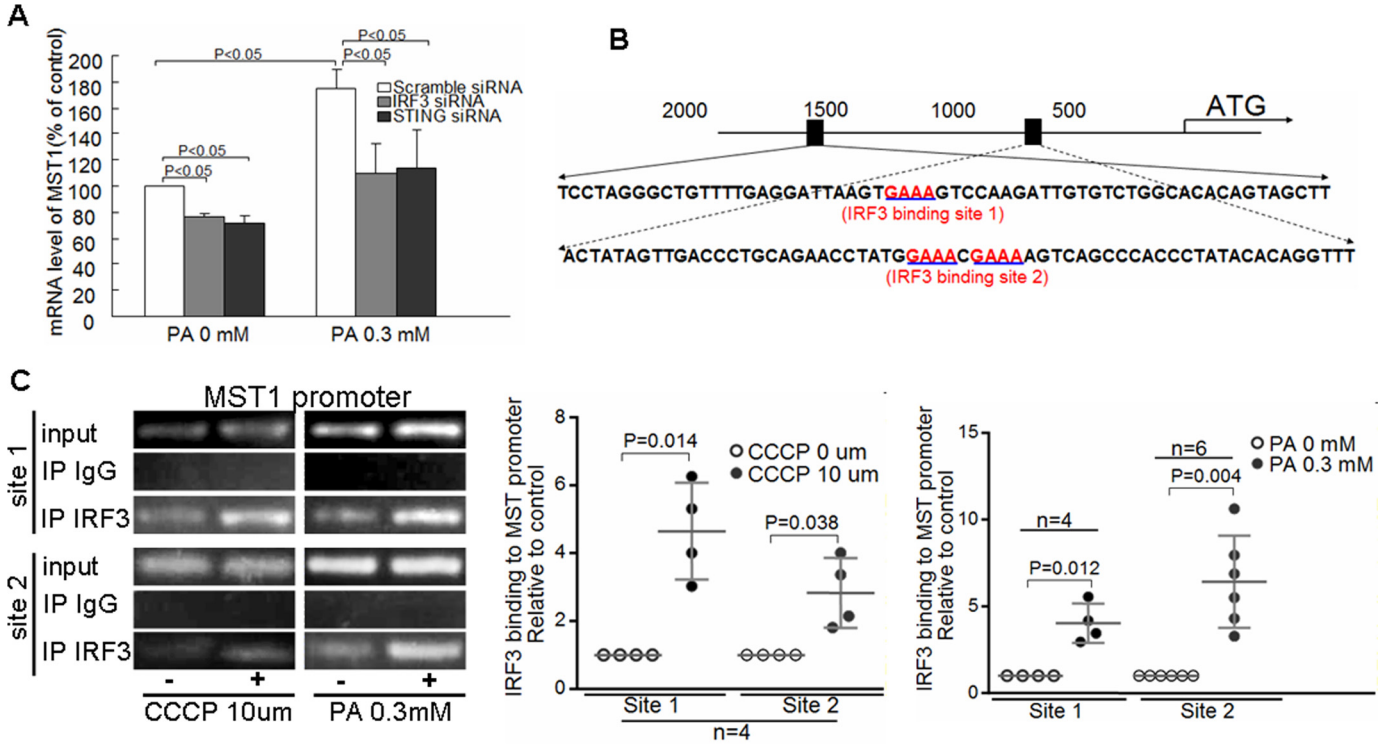

Figure 6. IRF3 directly binds to the MST1 promoter and mediates PA-induced induction of MST1 expression. *A,* HAECs were transfected with scramble siRNA, IRF3 siRNA, or STING siRNA and then treated with PA for 24 h. RT-PCR analysis showed that PA treatment increased MST1 mRNA, which can be prevented by knocking down IRF3 or STING ($n = 6$ biological repeats). *B,* putative IRF3-binding sites upstream of the 5′ UTR of the *MST1* gene are shown. *C,* HAECs were treated with PA or CCCP for 24 h. Chromatin immunoprecipitation assay showed that IRF3 bound to the *MST1* gene promoter. The binding was increased in PA or CCCP-treated cells ($n = 4$ biological repeats).

for Hippo pathway activation and YAP inhibition. We found that the cGAS–STING–IRF3 pathway was involved in dysregulation of the Hippo–YAP pathway in endothelial cells. IRF3 directly bound to the MST1 promoter and induced MST1 expression, leading to YAP phosphorylation and inactivation, and angiogenesis inhibition. Interestingly, a recent study showed that MST1 directly phosphorylated and inactivated IRF3, reduced IRF3 dimerization, and DNA-binding and transcription activity (54). Thus, the cross-talk between the Hippo–YAP and the cGAS–STING–IRF3 pathways can be highly specific to factors such as cell types and stress conditions. Whether the cGAS–STING–IRF3 pathway can also activate Hippo–YAP signaling under other stimulators (*e.g.* hyperglycemia) or in other cells (*e.g.* inflammatory cells) remains to be determined.

The cGAS–STING–IRF3 pathway plays a critical role in the innate immune response by promoting the expression of genes that suppress pathogen replication or facilitate adaptive immunity (55, 56). Recent studies suggest that STING is also involved in inflammation (8, 57). Gain-of-function mutations in STING have been identified in an autoinflammatory disease characterized by early-onset systemic inflammation and vasculopathy (8) and in familial inflammatory syndrome (58). Here our *in vitro* study shows that activation of the STING pathway is also involved in metabolic stress-induced angiogenesis inhibition. However, further *in vivo* studies are needed to determine whether this pathway plays a role in angiogenesis defects in diabetes, or whether wound healing in the diabetic condition can be improved by genetic deletion or pharmacological inhibition of STING.

Conclusions

Our study has demonstrated that PA dysregulates the Hippo–YAP pathway and inhibits endothelial angiogenesis. PA induces mtDNA cytosolic release and activates the cytosolic DNA sensor cGAS–STING–IRF3 pathway, which promotes MST1 expression, leading to inhibition of YAP and endothelial angiogenesis. This mechanism may have implications in impaired wound healing in diabetes.

Experimental procedures

Cell culture

Cells were cultured as described previously (27, 28). Primary HAECs was purchased from ScienCell Research Laboratories (CA) and cultured in endothelial cell medium (ScienCell Research Laboratories) supplemented with 5% fetal bovine serum, endothelial cell growth factors, and penicillin/streptomycin solution.

Figure 5. The cGAS–STING–IRF3 pathway mediates PA-induced MST1 up-regulation and YAP inhibition. HAECs were transfected with scramble siRNA or cGAS or STING or IRF3 siRNA and then treated with PA for 24 h. Western blot analysis showed that knocking down cGAS (*A*) or STING or IRF3 (*B*) prevented PA-induced activation MST1 expression and YAP phosphorylation ($n = 6$ biological repeats). *C,* representative images of immunostaining showed that knocking down STING or IRF3 prevented PA-induced YAP cytoplasm retention ($n = 6$ biological repeats).

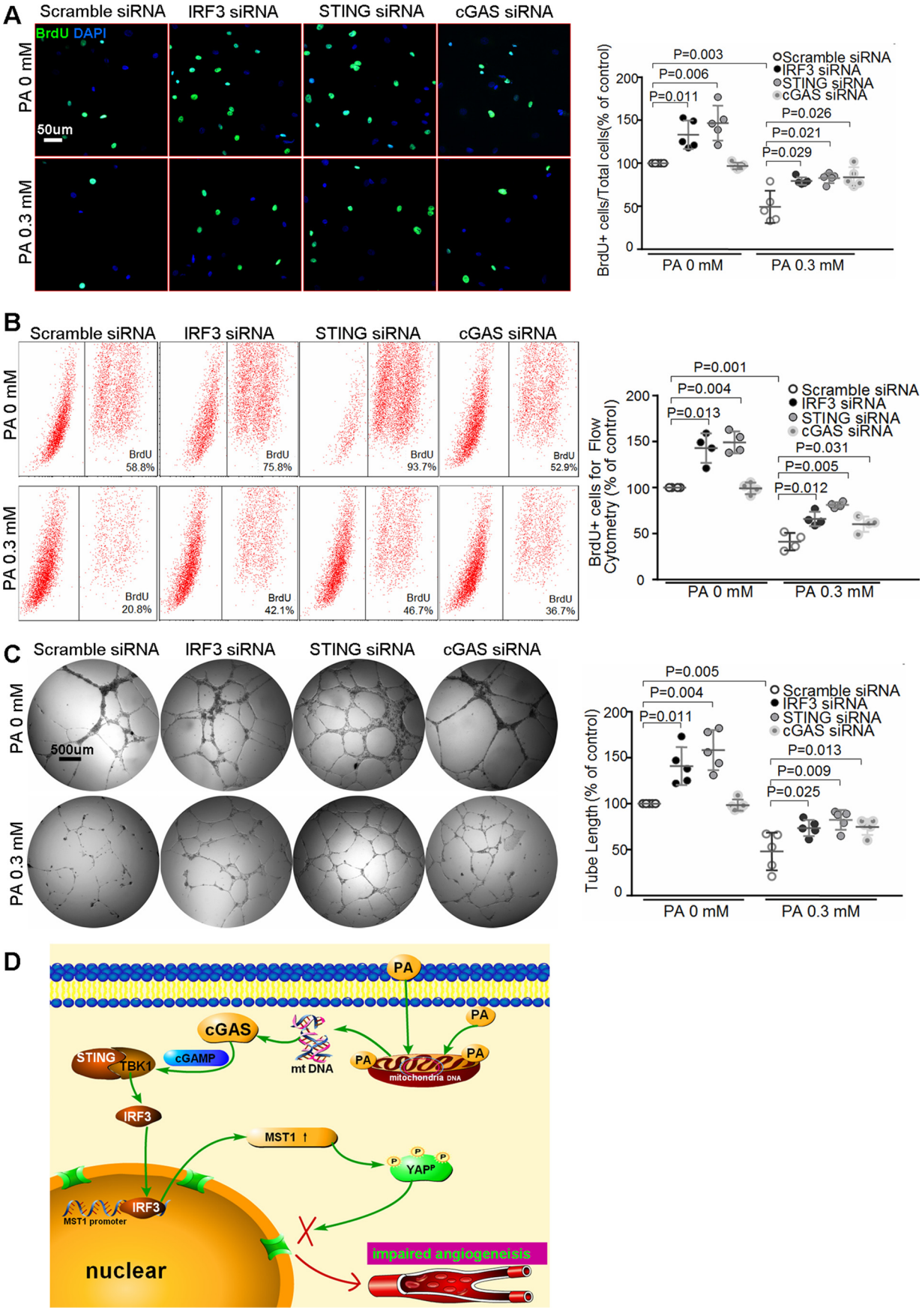
A
Scramble siRNA
IRF3 siRNA
STING siRNA
cGAS siRNA
BrdU DAPI
PA 0 mM
PA 0.3 mM
50um
BrdU+ cells/Total cells(% of control)
P=0.003
P=0.006
P=0.011
P=0.026
P=0.021
P=0.029
Scramble siRNA
IRF3 siRNA
STING siRNA
cGAS siRNA
PA 0 mM
PA 0.3 mM
B
Scramble siRNA
IRF3 siRNA
STING siRNA
cGAS siRNA
PA 0 mM
PA 0.3 mM
BrdU 58.8%
BrdU 75.8%
BrdU 93.7%
BrdU 52.9%
BrdU 20.8%
BrdU 42.1%
BrdU 46.7%
BrdU 36.7%
BrdU+ cells for Flow Cytometry (% of control)
P=0.001
P=0.004
P=0.013
P=0.031
P=0.005
P=0.012
Scramble siRNA
IRF3 siRNA
STING siRNA
cGAS siRNA
PA 0 mM
PA 0.3 mM
C
Scramble siRNA
IRF3 siRNA
STING siRNA
cGAS siRNA
PA 0 mM
PA 0.3 mM
500um
Tube Length (% of control)
P=0.005
P=0.004
P=0.011
P=0.013
P=0.009
P=0.025
Scramble siRNA
IRF3 siRNA
STING siRNA
cGAS siRNA
PA 0 mM
PA 0.3 mM
D
PA
cGAS
cGAMP
STING
TBK1
mt DNA
mitochondria DNA
IRF3
MST1 ↑
YAP
IRF3
MST1 promoter
nuclear
impaired angiogeneisis

Gene silencing or overexpression

YAP siRNA and MST1 siRNA were bought from RiboBio Co. (Guangzhou, China) and GenePharma Co. (Shanghai, China). cGAS siRNA, STING siRNA, and IRF3 siRNA were bought from Thermo Fisher Scientific Inc. (Shanghai, China), RiboBio Co. (Guangzhou, China), and GenePharma Co. (Shanghai, China). The best siRNA for each gene was selected and used in our study. pcDNA4/HisMaxB-YAP1-S127A (number 18988, Addgene) and pcDNA4/HisMaxB-YAP1 (number 18978, Addgene) were used in this study. HAECs were transfected with 0.5 μg of plasmids and then treated with PA for 24 h. Cell transfection was performed with Lipofectamine 2000 (12566014, Thermo Fisher Scientific Inc.), and for siRNA and Lipofectamine® 3000 transfection reagent (L3000015, Thermo Fisher Scientific Inc.) for overexpression according to the manufacturer's instructions.

Palmitic acid preparation and treatment

Saturated PA was used in this study. PA preparation and treatment were performed as described previously (27, 28, 59). Briefly, PA was dissolved in ethanol into a 200 mM solution, and combined with 20% free fatty acid-free BSA to produce stock solutions with different concentrations from 1 to 5 mM. These stock solutions were filter-sterilized and stored at −20 °C. A control solution containing ethanol and BSA was similarly prepared. For the experiments, fresh working solutions were prepared by diluting each stock solution (1:10) in the endothelial cell medium. The final BSA concentration was constant in all PA working solutions, whereas the PA to BSA ratio varied with the PA concentrations.

BrdU proliferation assay

5-Bromo-2-deoxyuridine (BrdU) was used to detect the rate of cell proliferation. HAECs with a confluence of 50–70% on coverslips in 24-well cell culture plates were treated with PA for 24 h and 10 μg/ml of BrdU during the last 6 h. The treated cells were washed with PBS, fixed in 4% polyformaldehyde at room temperature for 30 min, and permeabilized with 0.5% Triton X-100 for 10 min. The DNA was denatured with 2 mol/liter of HCl for 1 h and the solution was neutralized with 0.1 mol/liter of sodium borate (pH 8.3) for 20 min. The cells on the coverslips were blocked with 1% BSA at room temperature for 1 h, incubated with anti-BrdU antibody at 4 °C overnight, Alexa Fluor 488-conjugated secondary antibodies (1:500, Invitrogen) at room temperature for 1 h, and DAPI nuclear staining for 10 min. The cells were observed under a Nikon eclipse Ti and UltraVIEW VOX confocal microscope. BrdU+ cells and total cells in 5 randomly selected fields per sample were counted. The ratio of BrdU+ cells/total cells (%) was compared between the groups.

Flow cytometry of BrdU proliferation assay

Flow cytometry was used to quantify the BrdU proliferation assay (60). Briefly, cells were cultured in 6-well plates and 10 μg/ml of BrdU was added during the last 6 h. Cells were harvested by a 0.125% trypsin solution, centrifuged, and resuspended in PBS and fixed by shaking gently on a shaking table in 4% polyformaldehyde for 30 min at room temperature, then centrifuged at 1000 rpm for 10 min, and washed by PBS, permeabilized with 0.5% Triton X-100 for 10 min, after being washed. The DNA was denatured with 2 mol/liter of HCl for 1 h and the solution was neutralized with 0.1 mol/liter of sodium borate (pH 8.3) for 20 min. 1% BSA was added for 1 h at room temperature after PBS and cells were kept on a gently shaking table, then stained with anti-BrdU antibody (BU1/75 (ICR1)) (FITC) (ab74545, Abcam, ShangHai, China) cells at 4 °C overnight under shaking. Data were analyzed and shown by kaluza 1.5a and Flowjo 10.0.

Migration assay

Scratch assay was performed to evaluate cell migration. Briefly, HAECS with 100% confluence in 6-well plates were scratched with 200-μl pipette tips. At 4, 8, 12, and 24 h after scratch, the areas of the gap were imaged and measured using ImageJ software. The migrated area was calculated as the initial gap area subtracted by the current gap area. The migration was presented as the ratio of the migrated area/the initial gap area. The area of gap at each time point was compared between the groups.

Matrigel tube formation assay

Matrigel (354248, BD Biosciences, Corning, NY) was added to the wells of 96-well culture plates, and concentrated at 37 °C for 0.5–1 h. Treated HAECs were harvested and seeded into the Matrigel containing wells. The total tube length were recorded at 4 and 12 h and calculated by ImageJ.

Western blot analysis

Western blot analysis was performed as described before (27, 28, 59). Protein lysates were extracted from the treated cells, separated by SDS-polyacrylamide gels, and then transferred to the polyvinylidine fluoride membranes. The membranes blocked with antibodies were incubated at 4 °C overnight, the secondary horseradish peroxidase-labeled antibody was incubated for 1 h in room temperature, bands were photographed by Alpha FluorChem E system and analyzed by ImageJ. Primary antibodies used were anti-phospho-YAP (Ser-127) (rabbit mAb, 13008, CST Shanghai, China), anti-YAP (12395, CST Shanghai, China), anti-phospho-MST1/MST2 (T180/T183) antibody (ab76323, Abcam, Shanghai, China), anti-MST1 antibody (ab51134, Abcam), anti-STING antibody (ab131604,

Figure 7. cGAS–STING–IRF3 signaling is involved in PA-induced inhibition of endothelial angiogenesis. HAECs were transfected with scramble siRNA, cGAS siRNA, STING siRNA, or IRF3 siRNA, and then treated with PA for 24 h. *A* and *B,* representative images ($n = 5$ biological repeats) (*A*) and flow cytometry analysis ($n = 4$ biological repeats) (*B*) of the BrdU proliferation assay showed that silencing cGAS, STING, or IRF3 prevented PA-induced inhibition of endothelial proliferation. *C,* tube formation assay showed that knocking down cGAS, STING, or IRF3 reversed PA-induced inhibition of endothelial angiogenesis ($n = 5$ biological repeats). *D,* proposed mechanism of PA-induced inhibition of angiogenesis. PA causes mitochondrial damage and cytosolic release of mtDNA, which is converted to cGAMP by cGAS. cGAMP activates STING, which facilitates TBK-1-mediated IRF3 phosphorylation/activation. Activated IRF3 enters the nucleus, binds to the *MST1* promoter, and induces MST1 expression. MST1 promotes YAP phosphorylation and cytosolic retention, leading to inhibition of endothelial angiogenesis.

Abcam), anti-cGAS antibody (abf124, Millipore, Billerica, MA), anti-phospho-IRF3 (S386) antibody (ab76493, Abcam), and anti-IRF3 antibody (ab76409, Abcam).

Real-time quantitative RT-PCR

We use TRIzol and chloroform to extract total RNA from the treated cells, PrimeScript™ RT reagent Kit (RR037A, Takara) helps to reverse the RNA transcribed into cDNAs. Real-time PCR were tested and quantified using a CFX Connect™ Fluorescent quantitative PCR detection system. Sequences of primers are shown as supplemental Table S1.

Mitochondrial transmembrane potential determination

JC-1 (C2006, Beyotime, China) was used to measure mitochondrial transmembrane potential, the experiment was carried as described (37) following the manufacturer's instructions.

Measurement of mtDNA in the cytosol

The experiment was carried out as described previously (28, 36). In brief, cells were treated with PA, lysed in cell lysis buffer (Thermo Fisher, Foster City, CA), and centrifuged at 700 × *g* for 10 min at 4 °C to remove the nuclei and intact cells. The volume of the supernatant was normalized according to the protein concentration. The cell lysate was further centrifuged at 10,000 × *g* for 30 min at 4 °C to isolate the cytosolic fraction, and then the DNA in the cytosolic fraction was isolated. The mtDNA was detected by quantitative PCR by using sequences in the gene coding for mitochondrial cytochrome *c* oxidase 1 (mtCOI) as primers. The nuclear DNA was measured by PCR by using sequences in the 18S rDNA (coding 18S ribosomal RNA) as primers. The copy numbers of mtDNA were normalized against the copy numbers of nuclear DNA. The primers for 18S rDNA were 5′-TAGAGGGACAAGTGGCGTTC-3′ (forward) and 5′-CGCTGAGCCAGTCAGTGT-3′ (reverse). The primers for human mtCOI were 5′-GCCCCCGATATGGCGTTT-3′ (forward) and 5′-GTTCAACCTGTTCCTGCTCC-3′ (reverse). The fluorescent quantitative PCR detection system CFX Connect™ helped to achieve the test.

Chromatin immunoprecipitation assay

We use the EZ-ChIP™ Kit (Merck Millipore) to complete this assay, the process was carried as described before (28) and following the manufacturer's protocol. In brief, PA-treated cells were first incubated with 1% formaldehyde at room temperature for 10 min, then ×10 glycine was added to quench the unreacted formaldehyde. The cells were then washed, harvested, and lysed. Cell lysates were sonicated and centrifuged to produce chromatin fragments 200–1000 base pairs in length. Then, the immunoprecipitation procedure was performed with an anti-IRF3 antibody (number 4302, CST) and protein A-agarose slurry (IgG served as the negative control). The immunocomplex beads were then washed sequentially with low-salt wash buffer, high-salt wash buffer, LiCl wash buffer, and Tris-EDTA buffer. The immunocomplex was eluted with elution buffer (100 mmol/liter of $NaHCO_3$, 1% SDS). The eluted immunocomplex and the input were incubated with 200 mM NaCl at 65 °C overnight and then incubated with proteinase K to digest the remaining proteins. The DNA was recovered by phenol/chloroform/isoamyl alcohol extraction and used as a template for PCR. Real-time quantitative PCR was performed to quantify the DNA, and the results were analyzed by using the comparative ΔC_t method. The size and purity of the PCR products were checked by analyzing the products with gel electrophoresis in 2% agarose gel. The sequences of primers that IRF3 binds to MST1 was shown in Fig. 6*B*.

Immunofluorescence and confocal imaging

The PA-treated cells were washed with PBS and fixed by 4% polyformaldehyde for 30 min at room temperature, and then permeabilized with 0.5% Triton X-100 for 10 min. 1% BSA was added to block the cells for 1 h at room temperature, and different antibodies were stained with cells at 4 °C for overnight. The cells was incubated with fluorescent-labeled secondary antibodies on the second day for 1 h and DAPI nuclear staining for 10 min at room temperature. For mitochondrial and cytolic DNA staining, before fixing cells, MitoTracker (M22426, Invitrogen) was added and incubated with cells for 30 min and anti-dsDNA antibody was used as the primary antibody. The cells were observed under Nikon eclipse Ti and UltraVIEW VOX confocal microscope. Primary antibodies used for immunostaining were: YAP antibody (1:200, number 12395, CST), STING antibody (1:100, number 13647, CST), IRF3 antibody (1:100, number 4302,CST), and dsDNA antibody (1:300, number ab27156, Abcam). Secondary antibodies used for immunostaining were: Alexa Fluor 488-conjugated secondary antibodies (1:500, A32723, Invitrogen) and Alexa Fluor 647-conjugated secondary antibodies (1:500, A32733 Thermo Fisher).

Statistical analysis

All quantitative variables are presented as the mean ± S.D. Two-group comparisons were performed by using the two sample *t* test. Multigroup comparisons were performed by using one-way analysis of variance. For all statistical analyses, two-tailed probability values were reported. $p < 0.05$ was considered statistically significant.

Author contributions—Y. H. S. and X. L. W. designed the study. L. S. Y. performed the experiments with assistance from W. L., Y. M., and W. W. W. L. S. Y., X. L. W., and Y. H. S. interpreted the results and wrote the manuscript, which was revised by all other authors.

References

1. Boulton, A. J., Vileikyte, L., Ragnarson-Tennvall, G., and Apelqvist, J. (2005) The global burden of diabetic foot disease. *Lancet* **366,** 1719–1724
2. Brem, H., and Tomic-Canic, M. (2007) Cellular and molecular basis of wound healing in diabetes. *J. Clin. Invest.* **117,** 1219–1222
3. Margolis, D. J., Hoffstad, O., Nafash, J., Leonard, C. E., Freeman, C. P., Hennessy, S., and Wiebe, D. J. (2011) Location, location, location: geographic clustering of lower-extremity amputation among Medicare beneficiaries with diabetes. *Diabetes Care* **34,** 2363–2367
4. Martin, P., and Parkhurst, S. M. (2004) Parallels between tissue repair and embryo morphogenesis. *Development* **131,** 3021–3034
5. Falanga, V. (2005) Wound healing and its impairment in the diabetic foot. *Lancet* **366,** 1736–1743
6. Gurtner, G. C., Werner, S., Barrandon, Y., and Longaker, M. T. (2008) Wound repair and regeneration. *Nature* **453,** 314–321

7. Sawada, N., Jiang, A., Takizawa, F., Safdar, A., Manika, A., Tesmenitsky, Y., Kang, K. T., Bischoff, J., Kalwa, H., Sartoretto, J. L., Kamei, Y., Benjamin, L. E., Watada, H., Ogawa, Y., Higashikuni, Y., *et al.* (2014) Endothelial PGC-1α mediates vascular dysfunction in diabetes. *Cell Metab.* **19,** 246–258
8. Liu, Y., Jesus, A. A., Marrero, B., Yang, D., Ramsey, S. E., Sanchez, G. A. M., Tenbrock, K., Wittkowski, H., Jones, O. Y., Kuehn, H. S., Lee, C. R., DiMattia, M. A., Cowen, E. W., Gonzalez, B., Palmer, I., *et al.* (2014) Activated STING in a vascular and pulmonary syndrome. *N. Engl. J. Med.* **371,** 507–518
9. Qi, W., Yang, C., Dai, Z., Che, D., Feng, J., Mao, Y., Cheng, R., Wang, Z., He, X., Zhou, T., Gu, X., Yan, L., Yang, X., Ma, J. X., and Gao, G. (2015) High levels of pigment epithelium-derived factor in diabetes impair wound healing through suppression of Wnt signaling. *Diabetes* **64,** 1407–1419
10. Larger, E., Marre, M., Corvol, P., and Gasc, J. M. (2004) Hyperglycemia-induced defects in angiogenesis in the chicken chorioallantoic membrane model. *Diabetes* **53,** 752–761
11. Dobler, D., Ahmed, N., Song, L., Eboigbodin, K. E., and Thornalley, P. J. (2006) Increased dicarbonyl metabolism in endothelial cells in hyperglycemia induces anoikis and impairs angiogenesis by RGD and GFOGER motif modification. *Diabetes* **55,** 19611069
12. D'Souza, D. R., Salib, M. M., Bennett, J., Mochin-Peters, M., Asrani, K., Goldblum, S. E., Renoud, K. J., Shapiro, P., and Passaniti, A. (2009) Hyperglycemia regulates RUNX2 activation and cellular wound healing through the aldose reductase polyol pathway. *J. Biol. Chem.* **284,** 17947–17955
13. Dunn, L. L., Simpson, P. J., Prosser, H. C., Lecce, L., Yuen, G. S., Buckle, A., Sieveking, D. P., Vanags, L. Z., Lim, P. R., Chow, R. W., Lam, Y. T., Clayton, Z., Bao, S., Davies, M. J., Stadler, N., *et al.* (2014) A critical role for thioredoxin-interacting protein in diabetes-related impairment of angiogenesis. *Diabetes* **63,** 675–687
14. Mehra, V. C., Jackson, E., Zhang, X. M., Jiang, X. C., Dobrucki, L. W., Yu, J., Bernatchez, P., Sinusas, A. J., Shulman, G. I., Sessa, W. C., Yarovinsky, T. O., and Bender, J. R. (2014) Ceramide-activated phosphatase mediates fatty acid-induced endothelial VEGF resistance and impaired angiogenesis. *Am. J. Pathol.* **184,** 1562–1576
15. Pan, D. (2010) The hippo signaling pathway in development and cancer. *Dev. Cell* **19,** 491–505
16. Zhao, B., Tumaneng, K., and Guan, K. L. (2011) The Hippo pathway in organ size control, tissue regeneration, and stem cell self-renewal. *Nat. Cell. Biol.* **13,** 877–883
17. Zhou, Q., Li, L., Zhao, B., and Guan, K. L. (2015) The hippo pathway in heart development, regeneration, and diseases. *Circ. Res.* **116,** 1431–1447
18. Yu, F. X., Zhao, B., and Guan, K. L. (2015) Hippo pathway in organ size control, tissue homeostasis, and cancer. *Cell* **163,** 811–828
19. Hong, A. W., Meng, Z., and Guan, K. L. (2016) The Hippo pathway in intestinal regeneration and disease. *Nat. Rev. Gastroenterol. Hepatol.* **13,** 324–337
20. Varelas, X. (2014) The Hippo pathway effectors TAZ and YAP in development, homeostasis and disease. *Development* **141,** 1614–1626
21. Choi, H. J., Zhang, H., Park, H., Choi, K. S., Lee, H. W., Agrawal, V., Kim, Y. M., and Kwon, Y. G. (2015) Yes-associated protein regulates endothelial cell contact-mediated expression of angiopoietin-2. *Nat. Commun.* **6,** 6943
22. Marti, P., Stein, C., Blumer, T., Abraham, Y., Dill, M. T., Pikiolek, M., Orsini, V., Jurisic, G., Megel, P., Makowska, Z., Agarinis, C., Tornillo, L., Bouwmeester, T., Ruffner, H., Bauer, A., *et al.* (2015) YAP promotes proliferation, chemoresistance, and angiogenesis in human cholangiocarcinoma through TEAD transcription factors. *Hepatology* **62,** 1497–1510
23. Elbediwy, A., Vincent-Mistiaen, Z. I., and Thompson, B. J. (2016) YAP and TAZ in epithelial stem cells: a sensor for cell polarity, mechanical forces and tissue damage. *Bioessays* **38,** 644–653
24. Vessby, B. (2003) Dietary fat, fatty acid composition in plasma and the metabolic syndrome. *Curr. Opin. Lipidol.* **14,** 15–19
25. Meng, Z., Moroishi, T., and Guan, K. L. (2016) Mechanisms of Hippo pathway regulation. *Genes Dev.* **30,** 1–17
26. Schrauwen, P., and Hesselink, M. K. (2004) Oxidative capacity, lipotoxicity, and mitochondrial damage in type 2 diabetes. *Diabetes* **53,** 1412–1417
27. Wu, W., Xu, H., Wang, Z., Mao, Y., Yuan, L., Luo, W., Cui, Z., Cui, T., Wang, X. L., and Shen, Y. H. (2015) PINK1-Parkin-mediated mitophagy protects mitochondrial integrity and prevents metabolic stress-induced endothelial injury. *PLoS ONE* **10,** e0132499
28. Mao, Y., Luo, W., Zhang, L., Wu, W., Yuan, L., Xu, H., Song, J., Fujiwara, K., Abe, J. I., LeMaire, S. A., Wang, X. L., and Shen, Y. H. (2017) STING-IRF3 triggers endothelial inflammation in response to free fatty acid-induced mitochondrial damage in diet-induced obesity. *Arterioscler. Thromb. Vasc. Biol.* **37,** 920–929
29. Ablasser, A., Goldeck, M., Cavlar, T., Deimling, T., Witte, G., Röhl, I., Hopfner, K. P., Ludwig, J., and Hornung, V. (2013) cGAS produces a 2′-5′-linked cyclic dinucleotide second messenger that activates STING. *Nature* **498,** 380–384
30. Sun, L., Wu, J., Du, F., Chen, X., and Chen, Z. J. (2013) Cyclic GMP-AMP synthase is a cytosolic DNA sensor that activates the type I interferon pathway. *Science* **339,** 786–791
31. Wu, J., Sun, L., Chen, X., Du, F., Shi, H., Chen, C., and Chen, Z. J. (2013) Cyclic GMP-AMP is an endogenous second messenger in innate immune signaling by cytosolic DNA. *Science* **339,** 826–830
32. Tanaka, Y., and Chen, Z. J. (2012) STING specifies IRF3 phosphorylation by TBK1 in the cytosolic DNA signaling pathway. *Sci. Signal.* **5,** ra20
33. Bowie, A. (2012) The STING in the tail for cytosolic DNA-dependent activation of IRF3. *Sci. Signal.* **5,** pe9
34. Prantner, D., Perkins, D. J., Lai, W., Williams, M. S., Sharma, S., Fitzgerald, K. A., and Vogel, S. N. (2012) 5,6-Dimethylxanthenone-4-acetic acid (DMXAA) activates stimulator of interferon gene (STING)-dependent innate immune pathways and is regulated by mitochondrial membrane potential. *J. Biol. Chem.* **287,** 39776–39788
35. White, M. J., McArthur, K., Metcalf, D., Lane, R. M., Cambier, J. C., Herold, M. J., van Delft, M. F., Bedoui, S., Lessene, G., Ritchie, M. E., Huang, D. C., and Kile, B. T. (2014) Apoptotic caspases suppress mtDNA-induced STING-mediated type I IFN production. *Cell* **159,** 1549–1562
36. West, A. P., Khoury-Hanold, W., Staron, M., Tal, M. C., Pineda, C. M., Lang, S. M., Bestwick, M., Duguay, B. A., Raimundo, N., MacDuff, D. A., Kaech, S. M., Smiley, J. R., Means, R. E., Iwasaki, A., and Shadel, G. S. (2015) Mitochondrial DNA stress primes the antiviral innate immune response. *Nature* **520,** 553–557
37. He, L., Xiao, D., Feng, J., Yao, C., and Tang, L. (2017) Induction of apoptosis of liver cancer cells by nanosecond pulsed electric fields (nsPEFs). *Med. Oncol.* **34,** 24
38. Geng, J., Sun, X., Wang, P., Zhang, S., Wang, X., Wu, H., Hong, L., Xie, C., Li, X., Zhao, H., Liu, Q., Jiang, M., Chen, Q., Zhang, J., Li, Y., *et al.* (2015) Kinases Mst1 and Mst2 positively regulate phagocytic induction of reactive oxygen species and bactericidal activity. *Nat. Immunol.* **16,** 1142–1152
39. Kurz, A. R., Pruenster, M., Rohwedder, I., Ramadass, M., Schäfer, K., Harrison, U., Gouveia, G., Nussbaum, C., Immler, R., Wiessner, J. R., Margraf, A., Lim, D. S., Walzog, B., Dietzel, S., Moser, M., *et al.* (2016) MST1-dependent vesicle trafficking regulates neutrophil transmigration through the vascular basement membrane. *J. Clin. Invest.* **126,** 4125–4139
40. Ishikawa, H., and Barber, G. N. (2008) STING is an endoplasmic reticulum adaptor that facilitates innate immune signalling. *Nature* **455,** 674–678
41. Singh, A., Ramesh, S., Cibi, D. M., Yun, L. S., Li, J., Li, L., Manderfield, L. J., Olson, E. N., Epstein, J. A., and Singh, M. K. (2016) Hippo signaling mediators Yap and Taz are required in the epicardium for coronary vasculature development. *Cell Rep.* **15,** 1384–1393
42. Moya, I. M., and Halder, G. (2016) The Hippo pathway in cellular reprogramming and regeneration of different organs. *Curr. Opin. Cell Biol.* **43,** 62–68
43. Pi, X., Xie, L., Portbury, A. L., Kumar, S., Lockyer, P., Li, X., and Patterson, C. (2014) NADPH oxidase-generated reactive oxygen species are required for stromal cell-derived factor-1α-stimulated angiogenesis. *Arterioscler. Thromb. Vasc. Biol.* **34,** 2023–2032
44. Vono, R., Fuoco, C., Testa, S., Pirrò, S., Maselli, D., Ferland McCollough, D., Sangalli, E., Pintus, G., Giordo, R., Finzi, G., Sessa, F., Cardani, R., Gotti, A., Losa, S., *et al.* (2016) Activation of the pro-Oxidant PKCβII-p66Shc signaling pathway contributes to pericyte dysfunction in skeletal muscles

of patients with diabetes with critical limb ischemia. *Diabetes* **65,** 3691–3704
45. Zhang, J., Li, L., Li, J., Liu, Y., Zhang, C. Y., Zhang, Y., and Zen, K. (2015) Protein tyrosine phosphatase 1B impairs diabetic wound healing through vascular endothelial growth factor receptor 2 dephosphorylation. *Arterioscler. Thromb. Vasc. Biol.* **35,** 163–174
46. Szendroedi, J., Phielix, E., and Roden, M. (2011) The role of mitochondria in insulin resistance and type 2 diabetes mellitus. *Nat. Rev. Endocrinol.* **8,** 92–103
47. Hesselink, M. K., Schrauwen-Hinderling, V., and Schrauwen, P. (2016) Skeletal muscle mitochondria as a target to prevent or treat type 2 diabetes mellitus. *Nat. Rev. Endocrinol.* **12,** 633–645
48. Green, D. R., Galluzzi, L., and Kroemer, G. (2014) Cell biology: metabolic control of cell death. *Science* **345,** 1250256
49. Madamanchi, N. R., and Runge, M. S. (2007) Mitochondrial dysfunction in atherosclerosis. *Circ. Res.* **100,** 460–473
50. Kluge, M. A., Fetterman, J. L., and Vita, J. A. (2013) Mitochondria and endothelial function. *Circ. Res.* **112,** 1171–1188
51. Fan, R., Kim, N. G., and Gumbiner, B. M. (2013) Regulation of Hippo pathway by mitogenic growth factors via phosphoinositide 3-kinase and phosphoinositide-dependent kinase-1. *Proc. Natl. Acad. Sci. U.S.A.* **110,** 2569–2574
52. Yin, F., Yu, J., Zheng, Y., Chen, Q., Zhang, N., and Pan, D. (2013) Spatial organization of Hippo signaling at the plasma membrane mediated by the tumor suppressor Merlin/NF2. *Cell* **154,** 1342–1355
53. Matsuda, T., Zhai, P., Sciarretta, S., Zhang, Y., Jeong, J. I., Ikeda, S., Park, J., Hsu, C. P., Tian, B., Pan, D., Sadoshima, J., and Del Re, D. P. (2016) NF2 activates Hippo signaling and promotes ischemia/reperfusion injury in the heart. *Circ. Res.* **119,** 596–606
54. Meng, F., Zhou, R., Wu, S., Zhang, Q., Jin, Q., Zhou, Y., Plouffe, S. W., Liu, S., Song, H., Xia, Z., Zhao, B., Ye, S., Feng, X. H., Guan, K. L., Zou, J., and Xu, P. (2016) Mst1 shuts off cytosolic antiviral defense through IRF3 phosphorylation. *Genes Dev.* **30,** 1086–1100
55. You, F., Wang, P., Yang, L., Yang, G., Zhao, Y. O., Qian, F., Walker, W., Sutton, R., Montgomery, R., Lin, R., Iwasaki, A., and Fikrig, E. (2013) ELF4 is critical for induction of type I interferon and the host antiviral response. *Nat. Immunol.* **14,** 1237–1246
56. Holm, C. K., Jensen, S. B., Jakobsen, M. R., Cheshenko, N., Horan, K. A., Moeller, H. B., Gonzalez-Dosal, R., Rasmussen, S. B., Christensen, M. H., Yarovinsky, T. O., Rixon, F. J., Herold, B. C., Fitzgerald, K. A., and Paludan, S. R. (2012) Virus-cell fusion as a trigger of innate immunity dependent on the adaptor STING. *Nat. Immunol.* **13,** 737–743
57. Ahn, J., Gutman, D., Saijo, S., and Barber, G. N. (2012) STING manifests self DNA-dependent inflammatory disease. *Proc. Natl. Acad. Sci. U.S.A.* **109,** 19386–19391
58. Jeremiah, N., Neven, B., Gentili, M., Callebaut, I., Maschalidi, S., Stolzenberg, M. C., Goudin, N., Frémond, M. L., Nitschke, P., Molina, T. J., Blanche, S., Picard, C., Rice, G. I., Crow, Y. J., Manel, N., Fischer, A., Bader-Meunier, B., and Rieux-Laucat, F. (2014) Inherited STING-activating mutation underlies a familial inflammatory syndrome with lupus-like manifestations. *J. Clin. Invest.* **124,** 5516–5520
59. Li, X. N., Song, J., Zhang, L., LeMaire, S. A., Hou, X., Zhang, C., Coselli, J. S., Chen, L., Wang, X. L., Zhang, Y., and Shen, Y. H. (2009) Activation of the AMPK-FOXO3 pathway reduces fatty acid-induced increase in intracellular reactive oxygen species by upregulating thioredoxin. *Diabetes* **58,** 2246–2257
60. Wu, J., Liu, S., Meng, H., Qu, T., Fu, S., Wang, Z., Yang, J., Jin, D., and Yu, B. (2017) Neuropeptide Y enhances proliferation and prevents apoptosis in rat bone marrow stromal cells in association with activation of the Wnt/β-catenin pathway *in vitro*. *Stem Cell Res.* **21,** 74–84